Journal of Applied Polymer Science

Copper Phthalocyanine Oligomer Grafted Acrylic Elastomer Nanocomposites with High Dielectric Constants

Ruonan Liu, Jingwen Wang, Qing Li, Shuqin Li, Su Zhang, Xuejiao Ding
Department of Materials Science and Engineering, College of Materials Science and Technology, Nanjing University of Aeronautics and Astronautics, 29 Yudao Street, Nanjing 210016, People's Republic of China
Correspondence to: J. W. Wang (E-mail: wjw_msc@nuaa.edu.cn)

ABSTRACT: For many applications of dielectric elastomer (DE) actuators, it is desirable to endow the DE with a high dielectric constant (ε), high breakdown field, and good flexibility. In this study, a high-ε nanocomposite acrylic elastomer (ACM)-*g*-copper phthalocyanine (CuPc) was fabricated, in which the CuPc oligomer was grafted onto the backbone of ACM. This grafted composite exhibited several benefits over the physically blended one. Transmission electron microscopy micrographs indicated that the size of the grafted CuPc was in the range 15–30 nm, which was more than 25 times smaller than that of the simply blended one. At room temperature, ε of ACM-*g*-CuPc (with 15 wt % CuPc) reached 303 at 100 Hz. The remarkable enhancement in the dielectric response could be attributed to the greatly strengthened exchange coupling effect and the Maxwell–Wagner–Sillars polarization mechanism.
 J. Appl. Polym. Sci. **2014**, *131*, 39975.

KEYWORDS: composites; dielectric properties; elastomers; films; grafting

Received 11 July 2013; accepted 15 September 2013
DOI: 10.1002/app.39975

INTRODUCTION

The dielectric elastomer (DE), a type of electronic electroactive polymer, is a material that can transform electric energy directly into mechanical work and produce large strains. On the basis of its outstanding merits, including its high electric energy density, large deformation ability, and flexibility, DE has become a desirable material for the applications of actuators.[1–3] Generally, a DE actuator is made up of a DE membrane and two compliant electrodes, which essentially form an elastic capacitor. In the actuated state under the effect of coulomb forces, the DE film compresses in the thickness direction and expands in the planar direction.

In recent years, polyurethane (PU), silicones, and acrylics have been interesting candidates as dielectric materials. Zhenyi M. et al.[4] observed an actuation strain of about 3% thermoplastic PU under an electric field of 20 MV/m. Pelrine et al.[5] found that silicone rubber exhibited an actuation strain of about 30%, and acrylic elastomer (ACM) produced a 100% actuation strain after a 300% equal biaxial prestretch.[6] Compared with PU and silicone rubber, ACM can yield extremely large strains.[7] However, because of its low dielectric constant (ε), the driving electric field is generally more than 100 MV/m. For DE actuators, a high applied electric field would increase the weight and decrease the reliability and security; this is disadvantageous for practical applications. Because the energy density of a capacitor is determined by its ε and the square of electric field, increasing ε to get large strains in a low electric field is achievable, and the decreased applied electric field would bring DE actuators a more prospective future in the field of micro air vehicles, toys, and optical devices.

For several years, both experimental and theoretical studies have been carried out to increase the ε values of polymers, in which the addition of various high-ε fillers into polymers have found great success.[8–11] Inorganic fillers such as ceramics possess a high elastic modulus, which is much higher than that of polymers, so their resulting composites usually suffer from a loss of flexibility and processability. On the contrary, composites with organic fillers have shown increased εs and good flexibility and processability. Among the organic fillers that have been used, copper phthalocyanine (CuPc) oligomer, a planar multi-ring organic semiconductor, exhibits a high ε ($>10^5$). The chemical structure of CuPc is shown in Scheme 1. Because of its giant conjugated structure, the nomadic polarization mechanism increases ε significantly. Nomadic polarization is a type of electrical polarization that can arise in a pure homogeneous molecular or crystalline solid under circumstances of the presence of an appreciable number of freed charges and long domains in

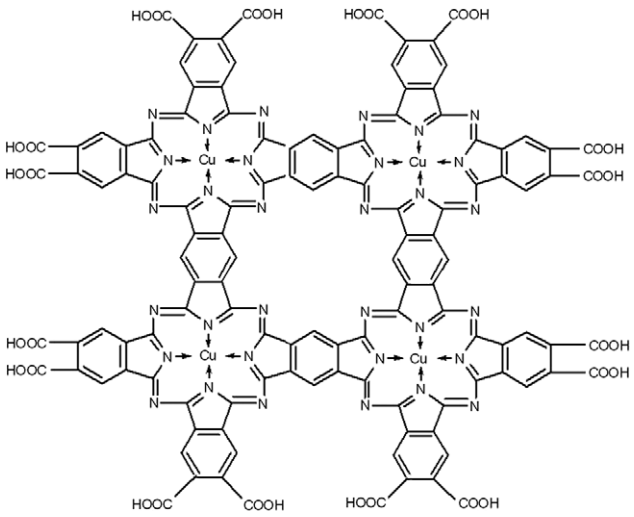

Scheme 1. Chemical structure of the CuPc oligomer.

which they can move under the influence of an external electric field.[12] However, the molecular stacking of CuPc macrocycles allows intermolecular interaction, which results in a large electrical conductivity so that the oligomer suffers from a high dielectric loss. Theoretically, when CuPc is dispersed into the polymer matrix, the polymer can provide an insulation layer around the CuPc particles to reduce the dielectric loss of the composite. However, because of the incompatibility between CuPc and the polymer matrix, CuPc molecules in the physically blended composite prefer to accumulate and then form conductive paths; this would reduce the breakdown field and increase the dielectric loss.[13,14] To overcome this issue, enhancing the compatibility to reduce the size of filler particles in the composite is an effective method. Additionally, small-sized CuPc particles can substantially strengthen the exchange coupling effect and increase ε of the composite.[15]

Technically, in polymeric composites, the compatibility between the filler and the polymer matrix can be enhanced by adding dispersant,[16] forming intermolecular hydrogen bonding,[17–19] cross-linking and grafting.[20] Recently, Wang et al.[21] reported a three-phase composite approach, acidified graphite nanosheets (AGS) /CuPc/PVDF, where AGS mixed CuPc particles were dispersed in PVDF matrix. Because of the well-dispersed CuPc particles, the ε and dielectric loss of the composite were 327 and 0.63 at 10 kHz, respectively. However, with grafting as an example, it is hard for the CuPc oligomers to graft onto the backbone of common polymers directly. Therefore, the introduction of an intermediate group that can react with CuPc is necessary. In this article, we present a novel fabrication method for producing high-ε acrylic nanocomposites. Hydroxyl-attached ACM was synthesized, and by the connection of toluene diisocyanate (TDI), which has two highly reactive isocyanate groups that can react with both hydroxyl and carboxyl groups, the CuPc oligomer was successfully grafted onto the backbone of ACM. In ACM-*g*-CuPc, the CuPc oligomer was well-distributed in the polymer matrix, and the particle size was reduced significantly, which strengthened the exchange coupling effect. As a result, ε of the ACM-*g*-CuPc film (with 15 wt % CuPc) reached 303 at 100 Hz.

EXPERIMENTAL

Materials

The CuPc oligomer was synthesized according to a procedure reported in ref. 22. Butyl acrylate (BA) and styrene (St) were analytical grade and were washed with NaOH to remove inhibitors and distilled before use. Hydroxyethyl acrylate (HEA) was analytical grade and was purified with activated carbons. TDI was distilled before use. Benzoyl peroxide was recrystallized from methanol before use. Dimethylformamide (DMF) was analytical grade and was dried with CaH_2 followed by distillation *in vacuo* before use. Other reagents were analytical grade and were used without further purification.

Synthesis of ACM-*g*-CuPc

The ACM here was synthesized via radical polymerization. A 100-mL, three-necked, round-bottomed flask fitted with a magnetic stirrer, a thermometer, and an allihn condenser was used as the reactor. BA (2.4 g), St (1.4 g), HEA (0.2 g), and DMF (4 mL) were added to the reactor. After dissolution for 5 min, the solution was purged with nitrogen and added to 0.02 g of benzoyl peroxide. After the solution was heated to 100°C to react for 5 h, TDI was added. Then, we dripped 25 mL of a 15 wt % CuPc/DMF solution into the reactor and kept the temperature at 80°C for another 5 h. After DMF was removed by reduced-pressure distillation, the mixture was washed with methanol to eliminate unreacted monomers, CuPc oligomers, and other byproducts. The final product, ACM-*g*-CuPc, was dried *in vacuo* at 75°C for 12 h. Scheme 2 presents the synthetic route of ACM-*g*-CuPc.

Preparation of the Composite Films

The composite films were prepared by solution casting method, and the typical film thickness was about 45 μm. For the physical blending of ACM and the CuPc oligomer (ACM/CuPc), ACM and CuPc were fully dissolved in DMF, and the compound was ultrasonically stirred until CuPc and ACM were uniformly mixed. Afterward, the solution was cast onto a polytetrafluoroethylene mold and kept in air at 70°C for 12 h. Then, the blend was annealed at 120°C *in vacuo* for another 12 h and slowly cooled to room temperature. For the ACM-*g*-CuPc film, the synthesized composite was used directly and the later procedure was the same as used for the preparation of the ACM/CuPc film.

Instrumentation

IR spectra were recorded with a Nicolet Nexus-670 Fourier transform infrared (FTIR) spectrometer with KBr as the background. ^{1}H-NMR spectra were carried out by a Bruker DRX-500 spectrometer with chloroform-*d* as the solvent. Specimens for inductively coupled plasma atomic emission spectrometry were

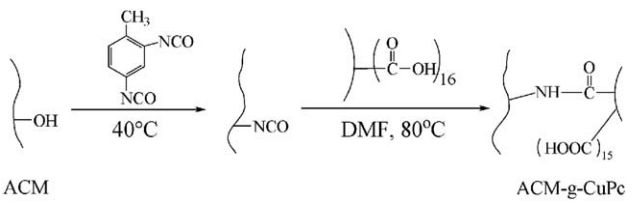

Scheme 2. Synthetic route of ACM-*g*-CuPc.

decomposed with a mixed solution of 70% nitric acid and 70% perchloric acid at a volume ratio of 5:1. After all of the liquids were naturally evaporated, the organic components were burned up in a crucible. The residues were diluted to a 10 mL of solution by 5% nitric acid, and the metal contents were measured by a Jarrell-Ash J-A1100 instruments. Differential scanning calorimetry (DSC) and thermogravimetric analysis (TGA) were carried out with a Netzsch DSC 200F3 calorimeter. Samples ranging from 10 to 12 mg were sealed in Al_2O_3 pans and heated under a nitrogen atmosphere from room temperature to 600°C at a heating rate of 10°C/min. A JEOL JEM-100S transmission electron microscope was used to observe the morphology of the composites. The film samples were cut into thin slices about 60 nm thick with a diamond blade in an ultracut microtome and placed onto copper grids before observation. The elastic moduli of the samples were measured with a dynamic mechanical thermal analyzer (Rheometric Scientific, Inc., DMTA-V). An X-ray diffraction (XRD) study was carried out with a Bruker D8 Advance rotating anode X-ray generator with a copper target. The grain size (L_{hkl}) in the direction perpendicular to the crystal planes was estimated by the Scherrer equation:

$$L_{hkl}=\frac{0.89\lambda}{B\cos\theta} \quad (1)$$

where λ is the X-ray wavelength, B is the full width at half-maximum of the diffraction peak in 2θ, and θ is the peak angular position. An HP 4294A Impedance analyzer was used for the characterization of frequency-dependent dielectric properties. The films were cut into small pieces 5 × 5 mm^2, and circular carbon grease electrodes with a 1.5 mm radius were coated in the center on both side of each sample. The ε values of the composite films were calculated by a parallel-plate capacitor equation:

$$\varepsilon=\frac{Cd}{\varepsilon_0 A} \quad (2)$$

where C is the capacitance, ε_0 is the vacuum dielectric permittivity, A is the area of the electrode, and d is the thickness of the DE. In addition, there are various models that can be used to estimate the effective ε of the composite. Take mean field-type composite theory as an example, which is reliable when the size effect is not important.[23] It is hypothesized that the composites are random mixtures of an ACM matrix and nearly spherical inclusions of CuPc. The effective ε of the composite can be estimated with the following equation:

$$\varepsilon=\frac{2\varepsilon_1+\varepsilon_2-2c_2(\varepsilon_1-\varepsilon_2)}{2\varepsilon_1+\varepsilon_2+c_2(\varepsilon_1-\varepsilon_2)}\varepsilon_1 \quad (3)$$

where ε_1 and ε_2 are the dielectric constants of the polymer matrix and dielectric filler, respectively, and c_2 is the volume fraction of the filler. A DF1784L60001 direct-current stabilized power supply was used to apply voltage for the actuator at a fixed ramp rate of 25 V/s until electric breakdown occurred. The film was 300% equal biaxial prestrained and fixed on a circular frame with a diameter of 75 mm. A circular area (diameter = 30 mm) at the center of the prestrained film was coated with conductive carbon grease on both sides and connected to the direct-current voltage source by a thin metal wire. A video extensometer system was used to monitor the changes in the diameter of the electrode-coated area.

RESULTS AND DISCUSSION

Characterization of the ACM and ACM-*g*-CuPc

For the poly(butyl acrylate–styrene–hydroxyethyl acrylate) elastomer, BA played the role of a soft monomer, St acted as a hard monomer, and HEA was the functional monomer that provided hydroxyl groups to react with the intermediate groups for the modification reaction. However, on the ACM molecular chain, there were no reactive groups that could directly react with the carboxyl groups of CuPc. Because isocyanate groups could easily react with both hydroxyl and carboxyl groups, TDI was chosen to attach ACM with highly reactive isocyanate groups to realize the grafting reaction of CuPc onto the modified ACM. The FTIR spectra of ACM and ACM-*g*-CuPc are illustrated in Figure 1(a). According to the spectrograms, the characteristic peaks of ACM at 700, 1163, 1450, 1728, and 2958 cm^{-1} appeared in the ACM-*g*-CuPc spectrum as well. It was also observed that there were three new characteristic peaks in the spectrograms of ACM-*g*-CuPc: 1362, 1599, and 3433 cm^{-1}. These corresponded to the stretching vibrations of the amido-linked carbon–nitrogen bond, the bending vibrations, and the stretching vibrations of nitrogen–hydrogen bonds, respectively. The appearance of these three absorption peaks demonstrated that the CuPc was grafted successfully. Furthermore, from ^{1}H-NMR spectra, as shown in Figure 1(b), the resonance at 4.81 ppm in the spectrogram of ACM was assigned to the hydrogen of hydroxyl, which disappeared in ACM-*g*-CuPc spectra. In addition, the resonance at 8.012 ppm belonged to the active hydrogen of the nitrogen–hydrogen bond, which was generated from the grafting reaction. These peaks confirmed that the CuPc was grafted. According to the inductively coupled plasma atomic emission spectrometry analysis, we estimated that after the grafting reaction, 97.3% of the CuPc oligomer was successfully grafted onto the backbone of the modified ACM.

Microstructure of the Composites

Figure 2 displays the transmission electron microscopy (TEM) micrographs of ACM/CuPc and ACM-*g*-CuPc (both with 15 wt % CuPc). Obviously, the CuPc molecules in both composite samples were aggregated into particles. In particular, smaller and more uniformly sized particles were obtained in ACM-*g*-CuPc. The size of the grafted CuPc particles was in the range 15–30 nm, which was over 25 times smaller than that of the simply blended one. In ACM/CuPc, because of the incompatibility between the CuPc and ACM matrix, the particulates were agglomerated, and the size of the CuPc particles reached a value of 500 nm. However, in ACM-*g*-CuPc, the CuPc oligomer that grafted on the main chain played the role of a nucleation center, which further induced the growth of CuPc crystallites. As the pendent CuPc molecules were distributed separately along the ACM backbone, the size of crystallites was restricted by the accessibility of the adjacent CuPc molecules.

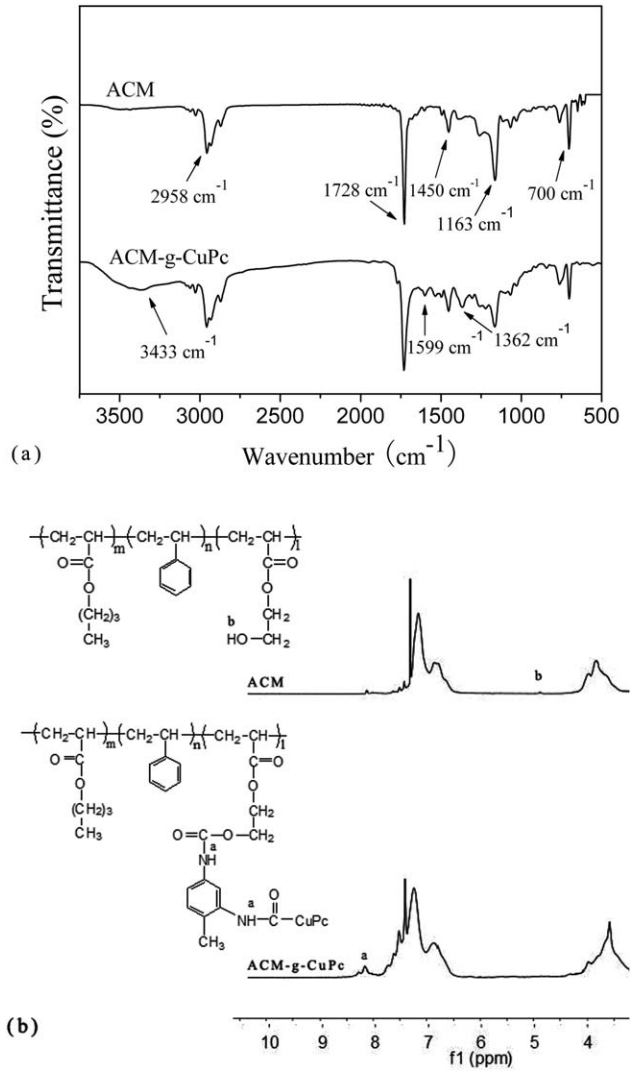

Figure 1. (a) FTIR and (b) ^{1}H-NMR spectra of pure ACM and ACM-*g*-CuPc.

Figure 3 presents the wide-angle XRD results of the pure ACM, ACM/CuPc, and ACM-*g*-CuPc acquired at room temperature. For pure ACM, the characteristic peak at 2θ (20.9°) indicated the amorphous structure of ACM, and the corresponding *d*-spacing was 4.25 Å, which was the length of an ACM unit.[24] For the composites, the presence of CuPc particles disturbed the ordered structure of the ACM molecule. As a result, the diffraction peak intensity of the composites at 20.9° was weakened sharply. The new diffraction peaks at 26.7° were the (021) reflection of the CuPc structure, and the diffraction peak intensity of the grafted composite was lower than that of the blended one. This may have been due to the fact that compared with ACM/CuPc, ACM-*g*-CuPc had more and smaller CuPc particles, and this impacted the microarea structure. As a result, the crystallinity of the CuPc molecules decreased.

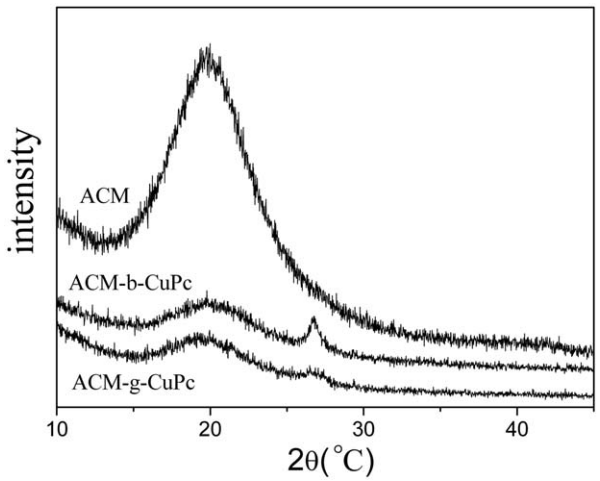

Figure 3. XRD results of the pure ACM, ACM/CuPc, and ACM-*g*-CuPc.

According to the Scherrer equation [eq. (1)], the grain size (L_{021}) of the composite samples was approximately 8.98 nm.

Thermal Behavior of the ACM and ACM-*g*-CuPc

The DSC thermograms of the pure ACM and the grafted composite, ACM-*g*-CuPc, are given in Figure 4. For pure ACM, the corresponding values of decomposition temperature (T_d) and the decomposition enthalpy (ΔH_d) were 413.2°C and 536.7 J/g, respectively. For ACM-*g*-CuPc, the values of T_d and ΔH_d were 412.0°C and 484.6 J/g. According to ref. 22, the degradation temperature of the CuPc oligomer was at least 660°C; this indicated that in the range of test temperatures, it was ACM rather than CuPc that degraded. Despite the content of CuPc in ACM-*g*-CuPc (15 wt % CuPc), the actual enthalpy of ACM in the

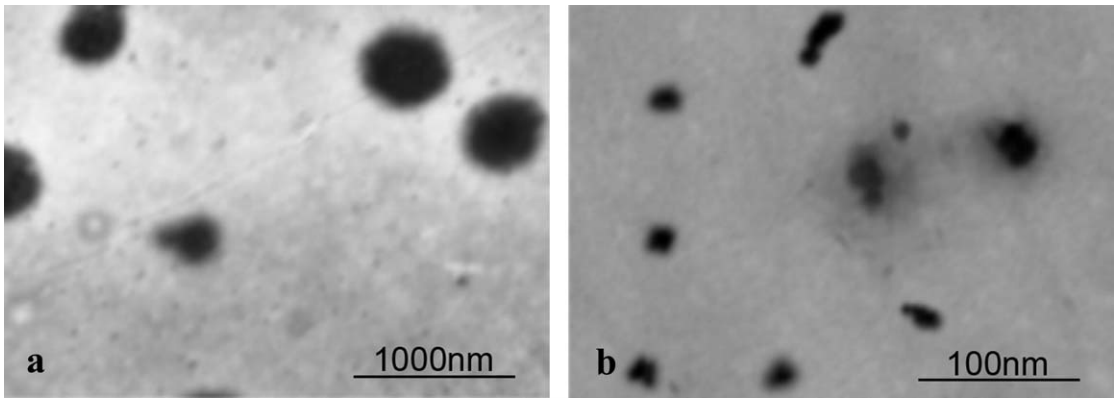

Figure 2. TEM photographs of (a) ACM/CuPc and (b) ACM-*g*-CuPc.

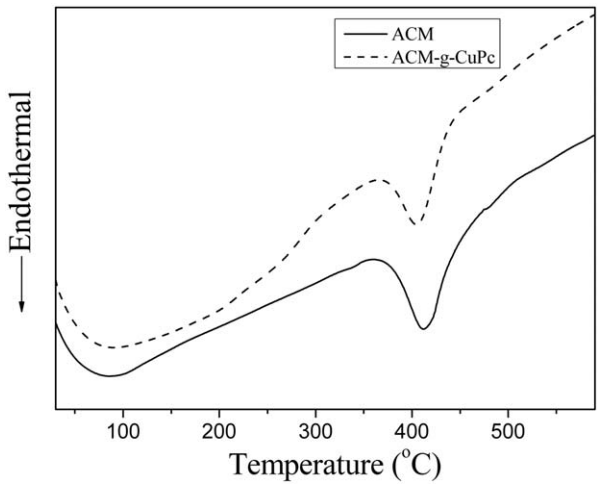

Figure 4. DSC curves of the pure ACM and ACM-*g*-CuPc.

composite corresponded to 570.1 J/g, which was higher than that of the pure ACM. This phenomenon may have been due to the grafting reaction, and this improved the homogeneity of CuPc in the ACM matrix and stabilized the molecular structure.

Figure 5 shows the TGA curves of the pure ACM and ACM-*g*-CuPc. The decomposition temperature at 5% weight loss [$T_{d(5\%)}$] was determined from the curves. For both the pure ACM and ACM-*g*-CuPc, at the temperatures around 50 to 300°C, there were slight weight losses, which corresponded to the decomposition of some small molecules, such as nonvolatile substances and oligomers. In the main decomposition stage, which began at 330°C for ACM and at 345°C for ACM-*g*-CuPc, the main chain of ACM degraded into a short-chain carbide, and the $T_{d(5\%)}$'s of ACM and ACM-*g*-CuPc occurred at 346 and 365°C, respectively. The weight loss of the pure ACM was 96.6%; this was much higher than that of ACM-*g*-CuPc, which was 75.3%. Despite the contribution of the CuPc oligomer (15 wt %), the weight loss and $T_{d(5\%)}$ of the ACM structure in the grafted composite was equivalent to 88.6% and 429°C, respectively. For ACM-*g*-CuPc, the increasing $T_{d(5\%)}$ and decreasing weight loss were attributed to its lightly crosslinked structure caused by the grafting reaction. The results of DSC and TGA demonstrated that the presence of CuPc improved the thermal stability of the grafted composite.

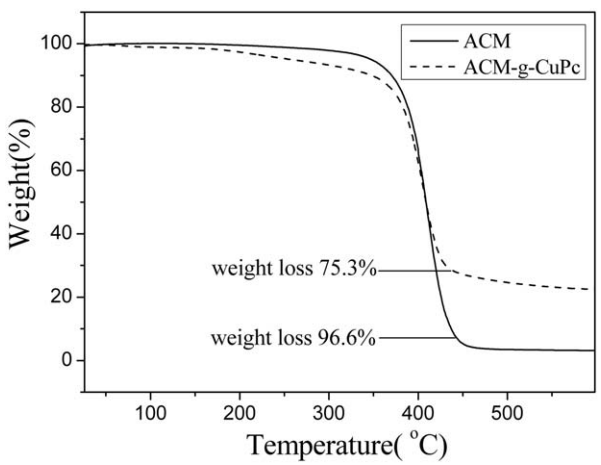

Figure 5. TGA thermograms of the pure ACM and ACM-*g*-CuPc.

Electrical and Mechanical Properties of the Composites

The dielectric properties as a function of the frequency ranged from 100 Hz to 1 MHz measured at room temperature for the grafted composite films with different CuPc contents are shown in Figure 6. The ε and dielectric loss decreased continuously as the frequency increased. This phenomenon indicated that the dielectric properties of the composites, especially those of the composites with high CuPc contents, had strong low-frequency dispersions; this was caused by the space-charge polarization mechanism in CuPc.[25] Furthermore, at low frequency, the ε and dielectric loss increased with increasing weight percentage of the CuPc oligomer. For example, at 100 Hz, the ε of ACM-*g*-CuPc with 5, 10, 15, and 20 wt % CuPc contents were 74, 192, 303, and 404, respectively. However, at frequencies above 3157, the ε of ACM-*g*−20% CuPc was even lower than that of the sample with 15 wt % CuPc. Because of all of these factors, the composite with 15 wt % CuPc content was the desired one for further research.

Figure 7 shows the dielectric properties of pure ACM, ACM/CuPc, and ACM-*g*-CuPc as a function of frequency from 100 Hz to 1 MHz as measured at room temperature. Compared with the pure ACM, the ε values of the composites was significantly increased, especially for ACM-*g*-CuPc, whose ε was as high as 303 at 100 Hz, which was nearly 60 times higher than that of the pure ACM (5.3).

In fact, the ε values of the CuPc-added composites were much higher than those derived from various models. According to eq. (3), ε_2 (4.3×10^5 for CuPc) was much higher than ε_1 (5.3 for ACM). After we simplified the previous equation, the final expression was obtained as follows:

$$\varepsilon = \frac{1+2c_2}{1-c_2}\varepsilon_1 \tag{4}$$

The value of ε was only 14 for both ACM-*g*-CuPc and ACM/CuPc. Clearly, the mean field-type composite theory could not explain the large enhancement in ε of the composites.

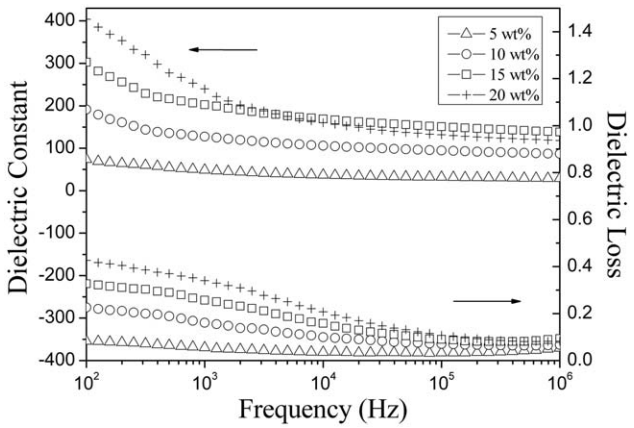

Figure 6. Dielectric properties of ACM-*g*-CuPc with different weight fractions of CuPc (5, 10, 15, and 20 wt %) measured at room temperature as a function of the frequency.

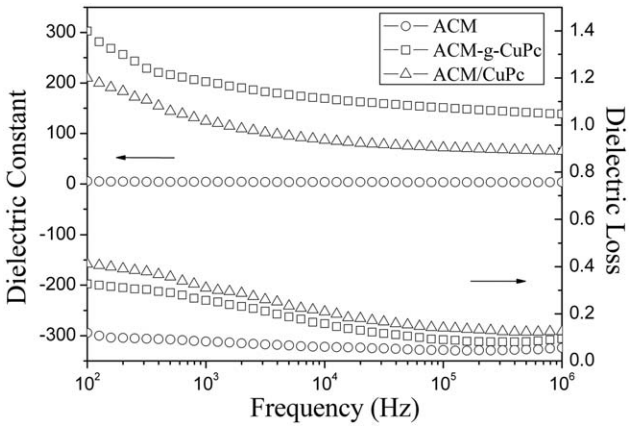

Figure 7. Dielectric properties of the pure ACM, ACM/CuPc, and ACM-*g*-CuPc, measured at room temperature as a function of the frequency from 100 Hz to 1 MHz.

Actually, the significant increasing of ε of the composites, especially for ACM-*g*-CuPc, was attributed to at least two reasons. First, the Maxwell–Wagner–Sillars space-charge polarization mechanism resulted in a strong, low-frequency dielectric dispersion; this often occurs in the system where large differences in the conductivity and ε exist between the two components. Second, the exchange coupling effect played a more important role.[26–28] As the composite became homogeneous, the exchange layer, where the polarization was strongly affected by both phases, eventually became the dominator when the heterogeneity size and exchange length became comparable.

Although the composites had the same CuPc contents, the ε of ACM-*g*-CuPc was much higher than that of ACM/CuPc (210). This was probably caused by the interfacial effect, which was derived from the much smaller CuPc particles, as observed in the TEM micrograms. In addition, the grafting reaction increased the number of branched chains. The higher the extent of branching was, the weaker the interaction force was, so the mobility of the molecular chains increased, and this enhanced the orientation polarization of the molecule. As a result, ε increased.

Along with the improvement in ε, the dielectric loss dropped as well. Take ACM−*g*−15%CuPc as an example; as shown in Figure 6 and 7, the dielectric loss was only 0.327. Although long-range intermolecular hopping of electrons made the CuPc suffer a high dielectric loss, the dielectric loss value of the composites was relatively low. In the composites, the ACM matrix played the role of insulation layers; this may have reduced the dielectric loss of the CuPc oligomer significantly. Moreover, because of the improved dispersion of the CuPc oligomer in the grafted composite, the dielectric loss of the ACM-*g*-CuPc was lower than that of ACM/CuPc.

The *actuation strain* (defined as the change in the diameter divided by the original diameter) of the ACM-*g*-CuPc (with 15 wt % CuPc) was 8.7% at 8.18 V/μm. The breakdown field of ACM-*g*-CuPc (with 15 wt % CuPc) was measured to be 30.5 V/μm, whereas the value of ACM/CuPc (with 15 wt % CuPc) was 20.6 V/μm. In ACM-*g*-CuPc, the size of the CuPc particles were substantially reduced (Figure 2), whereas in ACM/CuPc, the excessive agglomeration of CuPc particles easily formed conductive paths and lowered the breakdown field, so the breakdown field measured in ACM-*g*-CuPc was higher than that in ACM/CuPc.

The grafted composite not only had a good combination of high ε and low dielectric loss but also showed good flexibility. In this study, different contents of CuPc were grafted onto ACM to show their impact on the Young's modulus of the composites. According to the test results, the Young's modulus of pure ACM was 0.98 MPa, whereas the values of ACM-*g*-CuPc with 5, 10, and 15% CuPc contents were 1.5, 2.28, and 2.97 MPa, respectively. Although, the Young's modulus increased with increasing content of CuPc, the composite film with even 15 wt % CuPc was still very flexible.

CONCLUSIONS

ACM-*g*-CuPc, a flexible acrylic nanocomposite with a high ε was synthesized; in this nanocomposite, the CuPc oligomer was grafted onto the backbone of an isocyanate group modified polyacrylate matrix. Compared with the simple blended composites, the grafted composites showed better dielectric properties. The particle size of the grafted CuPc was in the range 15–30 nm. The DSC and TGA results showed that compared with the pure ACM, the thermal stability of the grafted composite was increased. More impressively, the ACM-*g*−15% CuPc film showed a high ε (303) accompanied by a low dielectric loss ($<$0.35). The remarkable enhancement in the dielectric response was attributed to the greatly strengthened exchange coupling effect and the Maxwell–Wagner–Sillars polarization mechanism.

ACKNOWLEDGMENTS

This work was supported by the National Natural Science Foundation of China (contract grant number 21174063), the Natural Science Foundation of Jiangsu Province (contract grant number BK20131358), and the Aeronautical Science Foundation of China (contract grant number 2011ZF52063).

REFERENCES

1. Araromi, O. A.; Conn, A. T.; Ling, C. S.; Rossiter, J. M.; Vaidyanathan, R.; Burgess, S. C. *Sens. Actuators A* **2011**, *167*, 459.
2. Brochu, P.; Pei, Q. B. *Macromol. Rapid Commun.* **2010**, *31*, 10.
3. Bozlar, M.; Punckt, C.; Korkut, S.; Zhu, J.; Foo, C. C.; Suo, Z. G.; Aksay, I. A. *Appl. Phys. Lett.* **2012**, *101*, 091907–1.
4. Zhenyi, M.; Scheinbeim, J. I.; Lee, J. W.; Newman, B. A. *J. Polym. Sci. Part B: Polym. Phys.* **1994**, *32*, 2721.
5. Pelrine, R. E.; Kornbluh, R. D.; Joseph, J. P. *Sens. Actuators A* **1998**, *64*, 77.
6. Pelrine, R.; Kornbluh, R.; Pei, Q. B.; Joseph, J. *Science* **2000**, *287*, 836.
7. Michel, S.; Zhang, X. Q.; Wissler, M.; Löwe, C.; Kovacs, G. *Polym. Int.* **2010**, *59*, 391.

8. Wang, J. W.; Wang, Y.; Wang, F.; Li, S. Q.; Xiao, J.; Shen, Q. D. *Polymer* **2009**, *50*, 679.
9. Zhang, Q. M.; Li, H. F.; Poh, M.; Xu, H. S.; Cheng, Z. Y.; Xia, F.; Huang, C. *Nature.* **2002**, *419*, 284.
10. Bai, Y.; Cheng, Z. Y.; Bharti, V.; Xu, H. S.; Zhang, Q. M. *Appl. Phys. Lett.* **2000**, *76*, 3804.
11. Wang, J. W.; Shen, Q. D.; Bao, H. M.; Yang, C. Z.; Zhang, Q. M. *Macromolecules* **2005**, *38*, 2247.
12. Norrell, C. J.; Pohl, H. A. *J. Polym. Sci. Part B: Polym. Phys.* **1974**, *12*, 913.
13. Wang, J. W.; Shen, Q. D.; Yang, C. Z. *Macromolecules* **2004**, *37*, 2294.
14. Huang, C.; Zhang, Q. M. *Adv. Mater.* **2005**, *17*, 1153.
15. Wang, J. W.; Wang, Y.; Li, S. Q.; Xiao, J. *J. Polym. Sci. Part B: Polym. Phys.* **2010**, *48*, 490.
16. Tasaki, K.; Gasa, J.; Wang, H. B.; DeSousa, R. *Polymer* **2007**, *48*, 4438.
17. Liu, G. Y.; Yang, X. L.; Wang, Y. M. *Polymer* **2007**, *48*, 4385.
18. Joshi, S. S.; Mebel, A. M. *Polymer* **2007**, *48*, 3893.
19. Tian, M.; Gao, Y.; Liu, Y.; Liao, Y. L.; Xu, R. W.; Hedin, N. E.; Fong, H. *Polymer* **2007**, *48*, 2720.
20. Zheng, Q. B.; Xue, Q. Z.; Yan, K. Y.; Gao, X. L.; Li, Q.; Hao, L. Z. *Polymer* **2008**, *49*, 800.
21. Wang, Q. T.; Jiang, W. L.; Guan, S. W.; Zhang, Y. H. *J Inorg. Organomet. Polym.* **2013**, *23*, 743.
22. Achar, B. N.; Fohlen, G. M.; Parker, J. A. *J. Polym. Sci. Part A: Polym. Chem.* **1982**, *20*, 1785.
23. Li, J. Y. *Phys. Rev. Lett.* **2003**, *90*, 217601–1.
24. Tangboriboon, N.; Wongpinthong, P.; Sirivat, A.; Kunanuruksapong, R. *Polym. Compos.* **2011**, *32*, 44.
25. Xu, H. S.; Bai, Y.; Bharti, V.; Cheng, Z. Y. *J. Appl. Polym. Sci.* **2001**, *82*, 70.
26. Seanor, D. A. In Electrical Properties of Polymers; Academic: New York, **1982**; Chapter *6*, p 242.
27. Bobnar, V.; Levstik, A.; Huang, C.; Zhang, Q. M. *Phys. Rev. Lett.* **2004**, *92*, 047604–1.
28. Bobnar, V.; Levstik, A.; Huang, C.; Zhang, Q. M. *Ferroelectrics* **2006**, *338*, 107.